AIR, WATER AND SOIL POLLUTION SCIENCE AND TECHNOLOGY

INDOOR AIR QUALITY

CONTROL, HEALTH IMPLICATIONS AND CHALLENGES

ROBERT M. RIDGWAY
EDITOR

NOVA

COMPLIMENTARY COPY

COMPLIMENTARY COPY

Air, Water and Soil Pollution Science and Technology

No part of this digital document may be reproduced, stored in a retrieval system or transmitted in any form or by any means. The publisher has taken reasonable care in the preparation of this digital document, but makes no expressed or implied warranty of any kind and assumes no responsibility for any errors or omissions. No liability is assumed for incidental or consequential damages in connection with or arising out of information contained herein. This digital document is sold with the clear understanding that the publisher is not engaged in rendering legal, medical or any other professional services.

COMPLIMENTARY COPY

Air, Water and Soil Pollution Science and Technology

Urban Air Pollution and Avenue Trees: Benefits, Interactions and Future Prospects
Abhijit Sarkar, PhD (Editor), Sujit Das
2021. ISBN: 978-1-68507-175-2 (Hardcover)
2021. ISBN: 978-1-68507-474-6 (eBook)

Soil Conservation: Strategies, Management and Challenges
António Avelino Batista Vieira (Editor),
António José Bento Gonçalves (Editor)
2021. ISBN: 978-1-53619-513-2 (Hardcover)
2021. ISBN: 978-1-53619-600-9 (eBook)

Air Pollution: Effects and Dangers
Jorge Esteban Colman Lerner (Editor)
2021. ISBN: 978-1-53619-544-6 (Hardcover)
2021. ISBN: 978-1-53619-556-9 (eBook)

Air Quality Observation in the U.S.: Systems, Needs, and Standards
Malcolm Parisi (Editor)
2014. ISBN: 978-1-63117-154-3 (Hardcover)
2014. ISBN: 978-1-63117-164-2 (eBook)

Air Quality: Environmental Indicators, Monitoring and Health Implications
Arthur Hermans (Editor)
2013. ISBN: 978-1-62808-259-3 (Hardcover)
2013. ISBN: 978-1-62808-260-9 (eBook)

More information about this series can be found at
https://novapublishers.com/product-category/series/air-water-and-soil-pollution-science-and-technology/

COMPLIMENTARY COPY

Robert M. Ridgway
Editor

Indoor Air Quality

Control, Health Implications and Challenges

nova
science publishers
www.novapublishers.com

COMPLIMENTARY COPY

Copyright © 2022 by Nova Science Publishers, Inc.

All rights reserved. No part of this book may be reproduced, stored in a retrieval system or transmitted in any form or by any means: electronic, electrostatic, magnetic, tape, mechanical photocopying, recording or otherwise without the written permission of the Publisher.

We have partnered with Copyright Clearance Center to make it easy for you to obtain permissions to reuse content from this publication. Simply navigate to this publication's page on Nova's website and locate the "Get Permission" button below the title description. This button is linked directly to the title's permission page on copyright.com. Alternatively, you can visit copyright.com and search by title, ISBN, or ISSN.

For further questions about using the service on copyright.com, please contact:
Copyright Clearance Center
Phone: +1-(978) 750-8400 Fax: +1-(978) 750-4470 E-mail: info@copyright.com.

NOTICE TO THE READER

The Publisher has taken reasonable care in the preparation of this book, but makes no expressed or implied warranty of any kind and assumes no responsibility for any errors or omissions. No liability is assumed for incidental or consequential damages in connection with or arising out of information contained in this book. The Publisher shall not be liable for any special, consequential, or exemplary damages resulting, in whole or in part, from the readers' use of, or reliance upon, this material. Any parts of this book based on government reports are so indicated and copyright is claimed for those parts to the extent applicable to compilations of such works.

Independent verification should be sought for any data, advice or recommendations contained in this book. In addition, no responsibility is assumed by the Publisher for any injury and/or damage to persons or property arising from any methods, products, instructions, ideas or otherwise contained in this publication.

This publication is designed to provide accurate and authoritative information with regard to the subject matter covered herein. It is sold with the clear understanding that the Publisher is not engaged in rendering legal or any other professional services. If legal or any other expert assistance is required, the services of a competent person should be sought. FROM A DECLARATION OF PARTICIPANTS JOINTLY ADOPTED BY A COMMITTEE OF THE AMERICAN BAR ASSOCIATION AND A COMMITTEE OF PUBLISHERS.

Additional color graphics may be available in the e-book version of this book.

Library of Congress Cataloging-in-Publication Data

ISBN: 979-8-88697-181-1 (e-book)

Published by Nova Science Publishers, Inc. † New York

COMPLIMENTARY COPY

Contents

COMPLIMENTARY COPY

Chapter 3

Computational Study and Experimental Validation of Heat Ventilation in a Box Prototype

Bdis Bakri[1], Slah Driss[2], Ahmed Ketata[2], Hani Benguesmia[3] and Zied Driss[2,*]

[1]Mechanical Engineering Department,
Faculty of Technology, University of M'sila, Algeria
[2]Laboratory of Electro-Mechanic Systems (LASEM),
National School of Engineers of Sfax (ENIS),
University of Sfax (US), Sfax, Tunisia
[3]LGE Laboratory,
Electrical Engineering Department,
Faculty of Technology,
University of M'sila, Algeria

Abstract

In this chapter, the impact of the numerical parameters on the heat ventilation was studied in a box prototype. Particularly, a computational study and an experimental validation have been developed to compare the standard k-ω turbulence model, the BSL k-ω turbulence model, the SST k-ω turbulence model, the standard k-ε turbulence model, the RNG k-ε turbulence model and the Realizable k-ε turbulence model. From the obtained results, it is noticed that the aerodynamic characteristics present the same emergence nevertheless the maximum values depend on the turbulence model. Particularly, it has been noted that the value founded with the standard k-ω turbulence model is nearest to the experimental

* Corresponding Author's Email: zied.driss@enis.tn.

In: Indoor Air Quality
Editor: Robert M. Ridgway
ISBN: 979-8-88697-134-7
© 2022 Nova Science Publishers, Inc.

COMPLIMENTARY COPY

results. This study tends to show that the standard k-ω turbulence model is the most efficient to study the air flow in the box prototype. For this model, the meshing effect on the CFD results was studied to choose the adequate mesh with a minimum calculated time. The numerical results were compared using experimental results developed in our laboratory. The good agreements confirm the numerical method.

Nomenclature

A_0	Model constant
A_s	Model constant
C_1	Model constant
$C_{1\varepsilon}$	Constant of the k-ε turbulence model (dimensionless)
$C_{2\varepsilon}$	Constant of the k-ε turbulence model (dimensionless)
C_μ	Constant of the k-ε turbulence model (dimensionless)
E	Total energy (J)
F_i	Force components on the i direction (N)
G_k	Generation of the turbulent kinetic energy ($kg.m^{-1}.s^{-3}$)
G_b	Generation of turbulence kinetic energy ($kg.m^{-1}.s^{-3}$)
G_v	Production of turbulent viscosity ($kg.m.s^{-2}$)
G_ω	Generation of the dissipation rate of the turbulent kinetic energy ($kg.m^{-1}.s^{-3}$)
H	Height (m)
h	Thermal enthalpy ($J.kg^{-1}$)
k	Turbulent kinetic energy ($m^2.s^{-2}$)
l	Length (m)
p	Pressure (Pa)
P_r	Prandt number
Q_H	Heat source or sink per unit volume ($kg.m^{-1}.s^{-3}$)
q_i	Diffusive heat flux (J)
Re	Reynolds number (dimensionless)
R_k	Constant of the k-ω turbulence model (dimensionless)
R_ω	Constant of the k-ω turbulence model (dimensionless)
S	Scalar measure of the deformation tensor
S_i	Mass-distributed ($kg.m^{-2}.s^{-2}$)
S_{ij}	Mean rate-of-strain tensor (s^{-1})
S_ω	Source terms of the specific dissipation rate of the turbulent kinetic energy ($kg.m^{-1}.s^{-3}$)

COMPLIMENTARY COPY

S_k	Source terms of the turbulent kinetic energy ($kg.m^{-1}.s^{-3}$)
S_ε	Source terms of the dissipation rate of the turbulent kinetic energy ($kg.m^{-1}.s^{-3}$)
T	Temperature (K)
t	Time (s)
u	Velocity components ($m.s^{-1}$)
u_i'	Fluctuating velocity components ($m.s^{-1}$)
V	Magnitude velocity ($m.s^{-1}$)
x_i	Cartesian coordinate (m)
x	Cartesian coordinate (m)
y	Cartesian coordinate (m)
Y_M	Fluctuating dilatation in compressible turbulence ($kg.m^{-1}.s^{-3}$)
Y_k	Turbulence dissipation of k
Y_ω	Turbulence dissipation of ω
z	Cartesian coordinate (m)
U	Free-stream velocity (m/s)
η_0	Constant of the k-ε turbulence model (dimensionless)
α_0	Constant of the k-ω turbulence model (dimensionless)
α_∞	Constant of the k-ω turbulence model (dimensionless)
α^*_∞	Constant of the k-ω turbulence model (dimensionless)
δ_{ij}	Kronecker delta function (dimensionless)
β	Constant of the k-ε turbulence model (dimensionless)
ε	Dissipation rate of the turbulent kinetic energy ($m^2.s^{-3}$)
μ	Dynamic viscosity (Pa.s)
μ_t	Turbulent viscosity (Pa.s)
μ_{eff}	Effective viscosity (Pa.s)
ω	Specific dissipation rate (s^{-1})
ρ	Density ($kg.m^{-3}$)
β_i	Constant of the k-ω turbulence model (dimensionless)
σ_k	Constant of the k-ε turbulence model (dimensionless)
σ_ε	Constant of the k-ε turbulence model (dimensionless)
σ_k	Turbulent Prandtl number for k (dimensionless)
σ_ω	Turbulent Prandtl number for ω (dimensionless)
τ_{ij}	Viscous shear stress tensor (Pa)
$(\tau_{ij})_{eff}$	Deviatoric stress tensor (Pa)
Φ	Equivalence ratio (dimensionless)
Γ_k	Effective diffusivity of k

COMPLIMENTARY COPY

Γ_ω	Effective diffusivity of ω
Ω	Swirl number (dimensionless)
Ω_{ij}	Rate of rotation tensor (s^{-1})

Keywords: heat ventilation, box prototype, turbulence model effect, experimental validation, CFD

1. Introduction

Heat ventilation by solar energy is used for wide range applications, such as hospitals, residential and commercial buildings. One of the chief benefits the solar ventilation is the reduction of the energy consumption by using renewable sources [1-7]. The mechanism of Heat ventilation has been investigated by many researchers. In particular, Driss et al. [1] investigated thermal comfort evaluation and the heat ventilation in a living room. In other applications, Teodosiu et al. [8] presented experimental-numerical comparisons to give the precision of a CFD model. Du et al. [9] conducted experimental measurements to present the characteristics of a Chinese house. Homod et al. [10] studied and proposed a new system by coupling reasons of internal conditions that are influenced by the outdoor environment. Terrados and Moreno [11] integrated the architectural concepts with energy efficient. Yasa [12] analysed the inside regions and the surrounding areas of education buildings and performed the microclimatic comfort. Premrov et al. [13] studied a single storey house wood frame case for objective to avoid the last energy. Johnston [14] predicted and measured performance of the building fabric in new build dwellings. Chan et al. [15] modeled a building of 21 floors by using Energy plus. The results of simulations indicate that the apartments flat presents satisfactory periods for the environment. Ibrahim et al. [16] planned technical coating projection. The proposed mathematical model was compared with experimental results. Nam and Chae [17] developed an optimal design of the grounding by using a numerical method. Alam et al. [18] improves a method of releasing heat from the building to reduce the energy demand of the building in a tropical environment. Rode [19] illustrated global relations to highlight the building performance. Han et al. [20] investigated hybrid solar energy system. A general view of the architectural envelope designs and innovative system was presented. Watson [21] reviewed design quality research on buildings in relation to users. Sailor et al. [22] describe the

COMPLIMENTARY COPY

system use implications that lead to building energy of green roof design decisions.

From these different anterior works, it has been noted that the design of buildings based on the reduction of the energy consumed. For thus, we have involved the study of the heat ventilation in a box prototype. Particularly, we have considered the turbulence models effect to choose the most effective model. The numerical results obtained in this work are validated via a box prototype realized in our LASEM laboratory.

2. Box Prototype System

Figure 1 depicts the physical domain of the considered box prototype. The box is characterized by a 0.22 m of height, 0.2 m of width and 0.3 m of length. Both square holes are localized at the same wall of the box. It has the same edge which is equal to 0.02 m, while it has different distance from the bottom wall of the box. The down hole is situated with a distance equal to $h_1 = 0.05$ m from the bottom wall, which is used to receive the air flow coming from the outside of the box prototype. However, the top hole is responsible on the evacuation of the air flow from the box to the surrounding air [1]. It is situated from the box base with a distance equal to $h_2 = 0.18$ m.

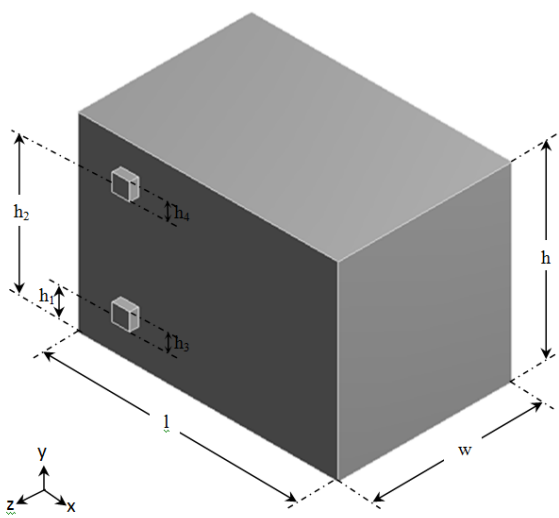

Figure 1. 3D view of the prototype.

COMPLIMENTARY COPY

3. Numerical Model

3.1. Boundary Conditions

The applied boundary conditions of the considered system are shown in Figure 2. The hot airflow enters to the box prototype through the down hole which is assumed as the inlet system. The velocity and the temperature at the inlet are respectively equal to V = 3.4 m.s-1 and T = 310 K. After the fluid recirculation inside the box, the airflow exits the system through a top hole with a pressure outlet value identical to the ambient static pressure. A no slip wall is applied for the outer walls of the domain.

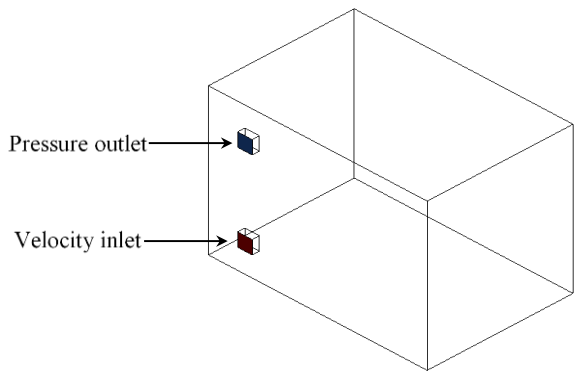

Figure 2. Boundary conditions.

3.2. Meshing

The meshing is an amportant step in the simulation procudure which affects directly the accuracy of the computantional findings. Then, a meshing analysis is required to minimize the error calculation. In the present study, the employed mesh density is taken from an anterior meshing analysis [23-32] which compares different meshing cases with our experimental data. The meshing choice is based on both accuracy and calculation time [33]. Figure 3 shows a view of the used optimal mesh with a tetrahedral volume cells. The 3D computantional domain is characterized by 167400 cells and 64312 nodes.

COMPLIMENTARY COPY

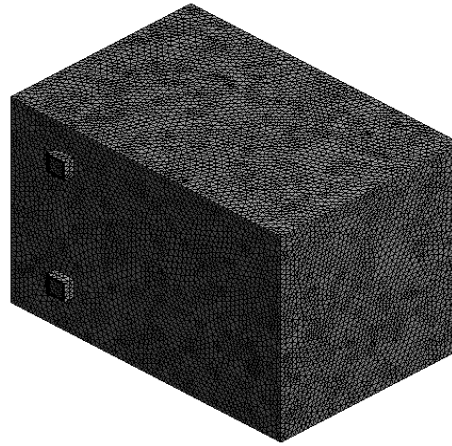

Figure 3. Meshing.

3.3. Mathematical Formulation

Table 1. Constants of the turbulence models

(a) Standard *k*-*ε* model

$C_{1\varepsilon}$	$C_{2\varepsilon}$	C_u	σ_k	σ_ε
1.44	1.92	0.09	1.0	1.3

(b) RNG *k*-*ε* model

C_1	$C_{2\varepsilon}$	β	..
1.44	1.92	0.012	4.38

(c) Realizable *k*-*ε* model

C_1	$C_{2\varepsilon}$	σ_k	σ_ε
1.44	1.9	1.0	1.2

(d) Standard *k*-*ω* model

α_0	α_∞	α^*_∞	R_ω	R_k	σ_k	σ_ω
1/9	1.9	1.0	2.95	6.0	2.0	2.0

COMPLIMENTARY COPY

Table 1. (Continued)

(e) BSL k-ω model

$\sigma_{k,1}$	$\sigma_{k,2}$	$\sigma_{\omega,1}$	$\sigma_{\omega,2}$	$\beta_{i,1}$	$\beta_{i,2}$
2.0	1.0	2.0	1.168	0.075	0.0828

(f) SST *k-ω* model

$\sigma_{k,1}$	$\sigma_{k,2}$	$\sigma_{\omega,1}$	$\sigma_{\omega,2}$	$\beta_{i,1}$	$\beta_{i,2}$	a_1
1.176	1.0	2.0	1.168	0.075	0.0828	0.31

The considered governing equations are the continuity equation, the momentum equations and the energy equation [34-26]. Taking a time average yields in the instantaneous equations, the Reynolds-averaged Navier-Stokes (RANS) equations can be written as follows:

$$\frac{\partial \rho}{\partial t} + \frac{\partial}{\partial x_i}(\rho u_i) = 0 \tag{1}$$

$$\frac{\partial}{\partial t}(\rho u_i) + \frac{\partial}{\partial x_j}(\rho u_i u_j) = -\frac{\partial p}{\partial x_j}\left[\mu\left(\frac{\partial u_i}{\partial x_j} + \frac{\partial j_i}{\partial x_i} - \frac{2}{3}\right)\right] + \frac{\partial}{\partial x_j}(-\rho \overline{u_i' u_j'}) F_i \tag{2}$$

To close equation (2), these Reynolds stresses $-\rho \overline{u_i' u_j'}$ must be modeled by using the Boussinesq hypothesis, written as follows:

$$-\rho \overline{u_i' u_j'} = \mu_t\left(\frac{\partial u_i}{\partial x_j} + \frac{\partial u_j}{\partial x_i}\right) - \frac{2}{3}\left(\rho k + \mu_t \frac{\partial u_k}{\partial x_k}\right)\delta_{ij} \tag{3}$$

The energy equation is expressed as follows:

$$\frac{\partial}{\partial t}(\rho E) + \frac{\partial}{\partial x_i}\left[u_i(\rho E + p)\right] = \frac{\partial}{\partial x_j}\left[\left(k + \frac{c_p \mu_t}{Pr_t}\right)\frac{\partial T}{\partial x_j} + u_i(\tau_{ij})_{eff}\right] + S_h \tag{4}$$

COMPLIMENTARY COPY

where K is the thermal conductivity and E is the total energy. $\left(\tau_{ij}\right)_{eff}$ is the deviatoric stress tensor and is written as follows:

$$\left(\tau_{ij}\right)_{eff} = \mu_{eff}\left(\frac{\partial u_j}{\partial x_i} + \frac{\partial u_i}{\partial x_j}\right) - \frac{2}{3}\mu_{eff}\frac{\partial u_k}{\partial x_k}\delta_{ij} \tag{5}$$

The standard model k-ε is modeling by both transport equations of the turbulent kinetic energy k and its dissipation rate ε. These equations are obtained from the following expressions:

$$\frac{\partial}{\partial t}(\rho k) + \frac{\partial}{\partial x_j}(\rho k u_i) = \frac{\partial}{\partial x_j}\left[\left(\mu + \frac{\mu_t}{\sigma_k}\right)\frac{\partial k}{\partial x_j}\right] + G_k + G_b - \rho\varepsilon - Y_M + S_k \tag{6}$$

$$\frac{\partial}{\partial t}(\rho\varepsilon) + \frac{\partial}{\partial x_i}(\rho\varepsilon u_i) = \frac{\partial}{\partial x_j}\left[\left(\mu + \frac{\mu_t}{\sigma_\varepsilon}\right)\frac{\partial \varepsilon}{\partial x_j}\right] + C_{1\varepsilon}\frac{\varepsilon}{k}\left(G_k + C_{3\varepsilon}G_b\right) - C_{2\varepsilon}\frac{\varepsilon^2}{k} + S_\varepsilon \tag{7}$$

μ_t is the turbulent viscosity computed from the combination of k and ε:

$$\mu_t = \rho\, C_\mu \frac{k^2}{\varepsilon} \tag{8}$$

Table 1 (a) illustrates the different constants employed in the k-ε turbulence model.

The RNG k-ε model presents similarity with the standard k-ε turbulence model:

$$\frac{\partial}{\partial t}(\rho k) + \frac{\partial}{\partial x_i}(\rho k u_i) = \frac{\partial}{\partial x_j}\left(\alpha_k \mu_{eff}\frac{\partial k}{\partial x_j}\right) + G_k + G_b - \rho\varepsilon - Y_M + S_k \tag{9}$$

$$\frac{\partial}{\partial t}(\rho\varepsilon) + \frac{\partial}{\partial x_i}(\rho\varepsilon u_i) = \frac{\partial}{\partial x_j}\left(\alpha_\varepsilon \mu_{eff}\frac{\partial \varepsilon}{\partial x_j}\right) + C_{1\varepsilon}\frac{\varepsilon}{k}\left(G_k + C_{3\varepsilon}G_b\right) - C_{2\varepsilon}\rho\frac{\varepsilon^2}{k} - R_\varepsilon + S_\varepsilon \tag{10}$$

COMPLIMENTARY COPY

In these conditions, we have to write:

$$d\left(\frac{\rho^2 k}{\sqrt{\varepsilon\mu}}\right)=1.72\,\frac{\hat{v}}{\sqrt{\hat{v}^3-1+C_v}}\,d\hat{v} \tag{11}$$

$$\hat{v}=\frac{\mu_{eff}}{\mu} \tag{12}$$

The difference between the RNG and the standard k-ε turbulence models consists in the addition of this term:

$$R_\varepsilon=\frac{C_\mu\rho\eta^3\left(1-\eta/\eta_0\right)}{1+\beta\eta^3}\frac{\varepsilon^3}{k} \tag{13}$$

where:

$$\eta=S\frac{k}{\varepsilon} \tag{14}$$

$$S=\sqrt{2S_{ij}S_{ij}} \tag{15}$$

Table 1 (b) illustrates the different constants employed in the RNG k-ε turbulence model.

In the realizable k-ε turbulence model, the transport equation is giving as follows:

$$\frac{\partial}{\partial t}(\rho k)+\frac{\partial}{\partial x_j}(\rho k u_j)=\frac{\partial}{\partial x_j}\left[\left(\mu+\frac{\mu_t}{\sigma_k}\right)\frac{\partial k}{\partial x_j}\right]+G_k+G_b-\rho\varepsilon-Y_M+S_k \tag{16}$$

$$\frac{\partial}{\partial t}(\rho\varepsilon)+\frac{\partial}{\partial x_j}(\rho\varepsilon u_j)=\frac{\partial}{\partial x_j}\left[\left(\mu+\frac{\mu_t}{\sigma_\varepsilon}\right)\frac{\partial\varepsilon}{\partial x_j}\right]+\rho C_1 S\varepsilon-\rho C_2\frac{\varepsilon^2}{k+\sqrt{v\varepsilon}}+C_{1\varepsilon}\frac{\varepsilon}{k}C_{3\varepsilon}G_b+S_\varepsilon \tag{17}$$

COMPLIMENTARY COPY

where:

$$C_1 = \max\left[0.43\frac{\eta}{\eta+5}\right] \tag{18}$$

As other k-ε turbulence models, the turbulent viscosity is calculated as follows:

$$\mu_t = \rho\, C_\mu \frac{k^2}{\varepsilon} \tag{19}$$

The difference between the realizable k-ε, the standard k-ε and the RNG k-ε turbulence models consists on the calculation of C_μ as:

$$C_\mu = \frac{1}{A_0 + A_s \frac{kU^*}{\varepsilon}} \tag{20}$$

Table 1 (c) illustrates the different constants employed in the realizable k-ε model.

In the k-ω standard turbulence model, the transport equations of the turbulent kinetic energy k and the specific dissipation rate ω are written as follows:

$$\frac{\partial}{\partial t}(\rho k) + \frac{\partial}{\partial x_i}(\rho k u_i) = \frac{\partial}{\partial x_j}\left(\Gamma_\omega \frac{\partial k}{\partial x_j}\right) + G_k + Y_k + S_k \tag{21}$$

$$\frac{\partial}{\partial t}(\rho \omega) + \frac{\partial}{\partial x_i}(\rho \omega u_i) = \frac{\partial}{\partial x_j}\left(\Gamma_\omega \frac{\partial k}{\partial x_j}\right) + G_\varpi + Y_\omega + S_\omega \tag{22}$$

Table 1 (d) illustrates the different constants employed in the k-ω turbulence model.

COMPLIMENTARY COPY

The BSL (Baseline) k-ω turbulence model presents a similar form:

$$\frac{\partial}{\partial t}(\rho k)+\frac{\partial}{\partial x_i}(\rho k u_i)=\frac{\partial}{\partial x_j}\left(\Gamma_k \frac{\partial k}{\partial x_j}\right)+G_k+Y_k+S_k \tag{23}$$

$$\frac{\partial}{\partial t}(\rho \omega)+\frac{\partial}{\partial x_i}(\rho \omega u_i)=\frac{\partial}{\partial x_j}\left(\Gamma_k \frac{\partial \omega}{\partial x_j}\right)+G_\omega+Y_\omega+D_\omega+S_\omega \tag{24}$$

Constants of the BSL k-ω model are presented in Table 1 (e).

Table 1 (e) illustrates the different constants of the BSL k-ω turbulence model.

To make the SST k-ω turbulence model more accurate, it includes all the refinements of the BSL k-ω turbulence model. Constants of the SST turbulence k-ω model are presented in Table 1 (f).

3.4. Choice of the Turbulence Model

The effect of the turbulence model on the numerical results have been studied in this section in order to achieve the adequate model. In fact, different turbulence models were studied using the software “Ansys Fluent 17.0” for solving the governing equations. Particularly, we have compared the BSL k-ω turbulence model, the standard k-ω turbulence model, the standard k-ε turbulence model, the SST k-ω turbulence model, the Realizable k-ε turbulence model and the RNG k-ε turbulence model. In the viewed direction set by the intersection of the two planes x = 0.06 m and z = -0.005 m, the superposition of the experimental results with the velocity profiles for the different turbulence models are presented in Figure 4. According to these results, the same profiles of the velocity have been observed and the values take down of the turbulence model. Particularly, it has been observed that the value founded with the experimental data is nearest to the standard k-ω tubulence model results. This study tends to show that the standard k-ω turbulence model is the most efficient to model the air flow in the present application. Therefore, the overall error designed between the numerical and the experimental data is equal to 5%. Thus, we found that the numerical results are in good agreement with the experimental data which confirms the validity of the numerical method.

COMPLIMENTARY COPY

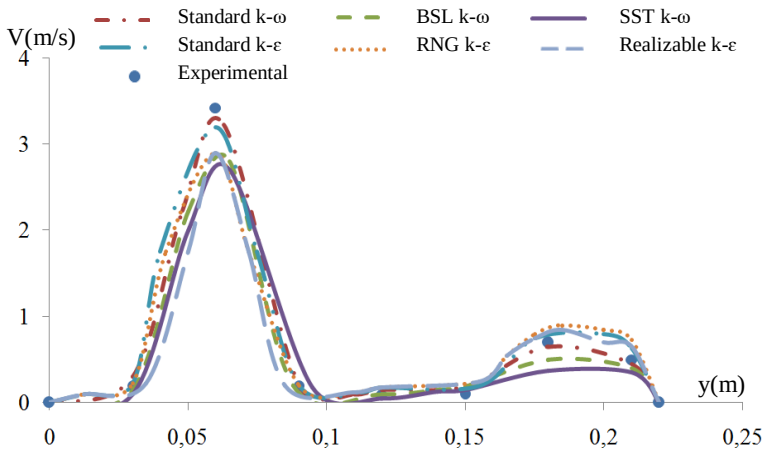

Figure 4. Velocity profiles in the direction defined by z = -0.005 m and x = 0.06 m.

4. Results and Discussion

The distribution of the velocity fields, the temperature, the total pressure, the turbulent kinetic energy and the turbulent viscosity are studied in this section. In the present study, the employed Reynolds number is equal to Re = 5100.

4.1. Velocity Fields

The distribution of the velocity fields in the plane defined by x = 0.06 m is shown in Figure 5 for the different studied turbulence models. From these results, it has been observed a discharge zone at the box inlet hole in all cases with average velocity equal to V = 3.4 $m.s^{-1}$. The inlet flow barges into the reverse wall of the box and then it moves inside the box with a turbulent behavior to evacuate through the top hole. Otherwise, both axial directions of the airflow are seen inside the box. The recirculation zone appeared in the whole area of the box is created by the change of the flow direction, specially by the first ascending flow. Meanwhile, the weak zone showed in the down area of the box is created by the second descending flow. In these conditions, the averaged velocity presents a very low value in the whole system when exclude the values in the discharge area which reaches V = 1.3 $m.s^{-1}$. The comparison between the different turbulence models affirms that the choice of

COMPLIMENTARY COPY

the adequate model presents a straight effect on the velocity fields. Particularly, it is noticed that the recirculation zone has been involved by the turbulence model choice. In this situation, the maximum value of the averaged velocity is obtained for the SST k-ω turbulence model and it reachs V = 4.75 $m.s^{-1}$. However, the minimum value is founded for the standard k-ε turbulence model and it reachs V = 4.42 $m.s^{-1}$.

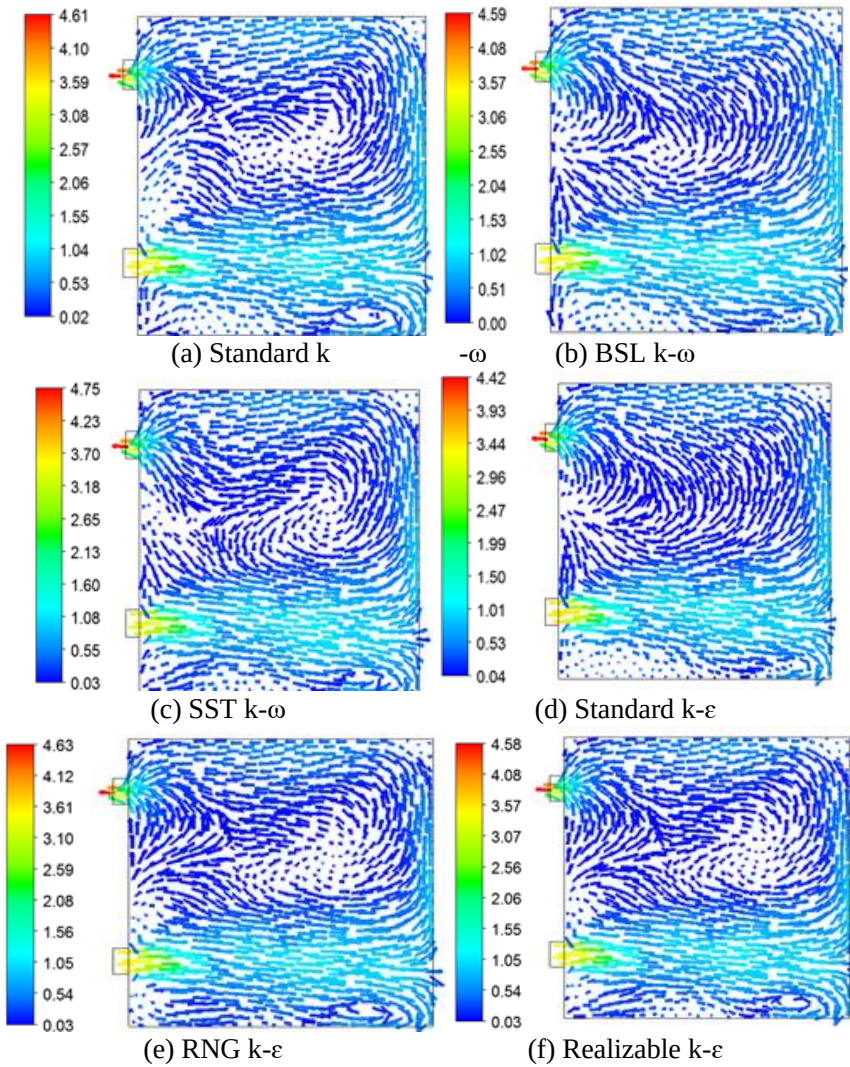

Figure 5. Velocity fields.

COMPLIMENTARY COPY

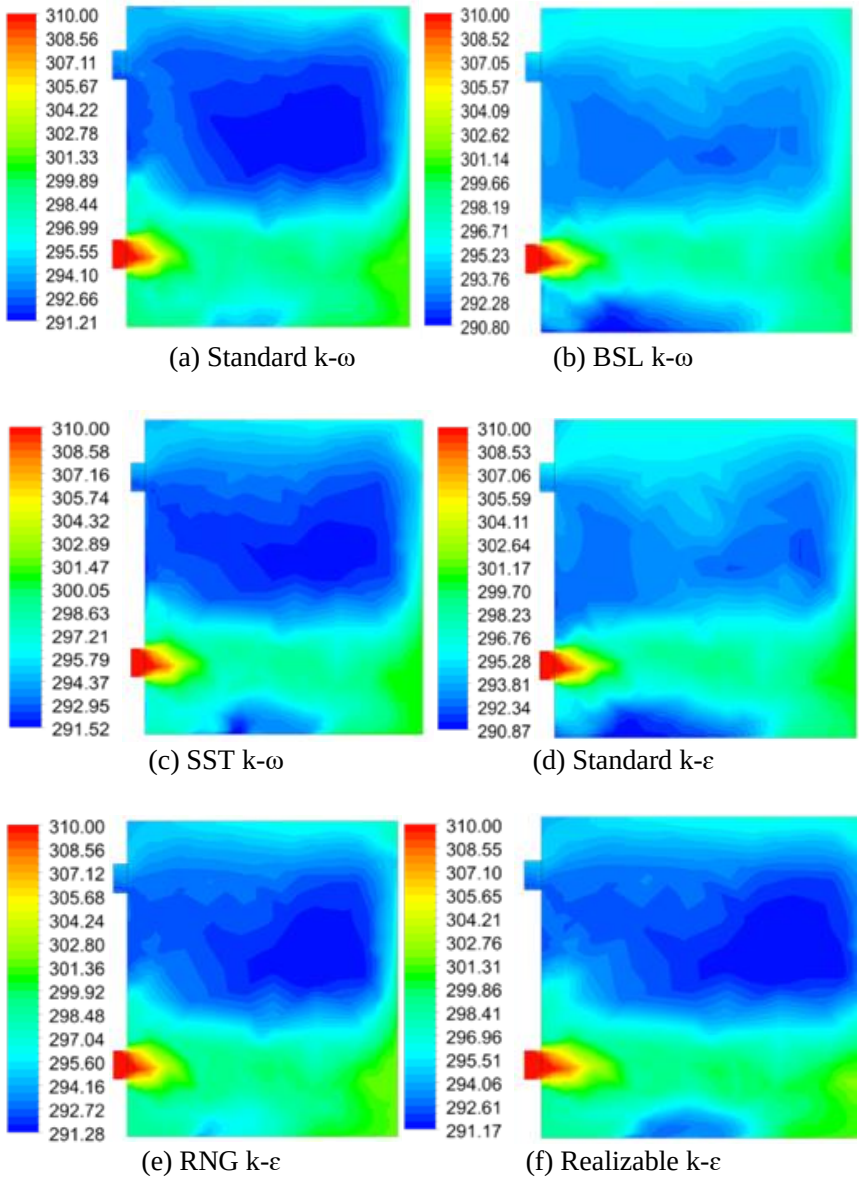

Figure 6. Distribution of the temperature.

COMPLIMENTARY COPY

4.2. Temperature

The distribution of the air temperature at t = 2 s and in the plane defined by x = 0.06 m is shown in Figure 6 for the considered turbulence models. According to these results, it has been observed that the temperature at the hole inlet is equal to T = 310 K while, it slightly decreases in the discharge area, at the hole inlet. However, the temperature decreases above the discharge area due to the recirculation region appeared into the whole area of the box prototype. Otherwise, the air temperature decreases gradually to reaches the minimum values at the system outlet with a value equal to T = 290 K. The comparison between the founded results affirms that the choice of the turbulence model presents a straight effect on the temperature distribution. Particularly, it has been noted that the minimum value of the temperature is obtained in the hole outlet for the BSL k-ω turbulence model and it is equal to T = 290.8 K. However, the maximum value of the temperature reaches T = 291.5 K for the SST k-ω turbulence model.

4.3. Total Pressure

Figure 7 shows the distribution of the total pressure in the plane defined by x = 0.06 m for all considered turbulence models. From these results, it is clear that a compression zone appears in the down hole of the box prototype for all cases. In fact, the total pressure decreases in the expulsion area, produced from the system inlet and attacked until the reverse wall of the box. This fact can be clarified by the recirculation zone showed at the whole area of the box prototype. From that point onward, the total pressure increases to reaches the peak value at the opposite wall. However, a depression zone is appeared at the top hole in the system outlet for all cases. A comparison between the different turbulence models gives that the turbulence model presents a straight effect on the distribution of the total pressure. In fact, it has been noted that the maximum value of the total pressure is founded for the standard k-ω and the SST k-ω turbulence models and presents a value equal to p = 101342 Pa. This value decreases slightly for the other turbulence models and reaches the minimum value equal to p = 101340 Pa, for the standard k-ε turbulence model.

COMPLIMENTARY COPY

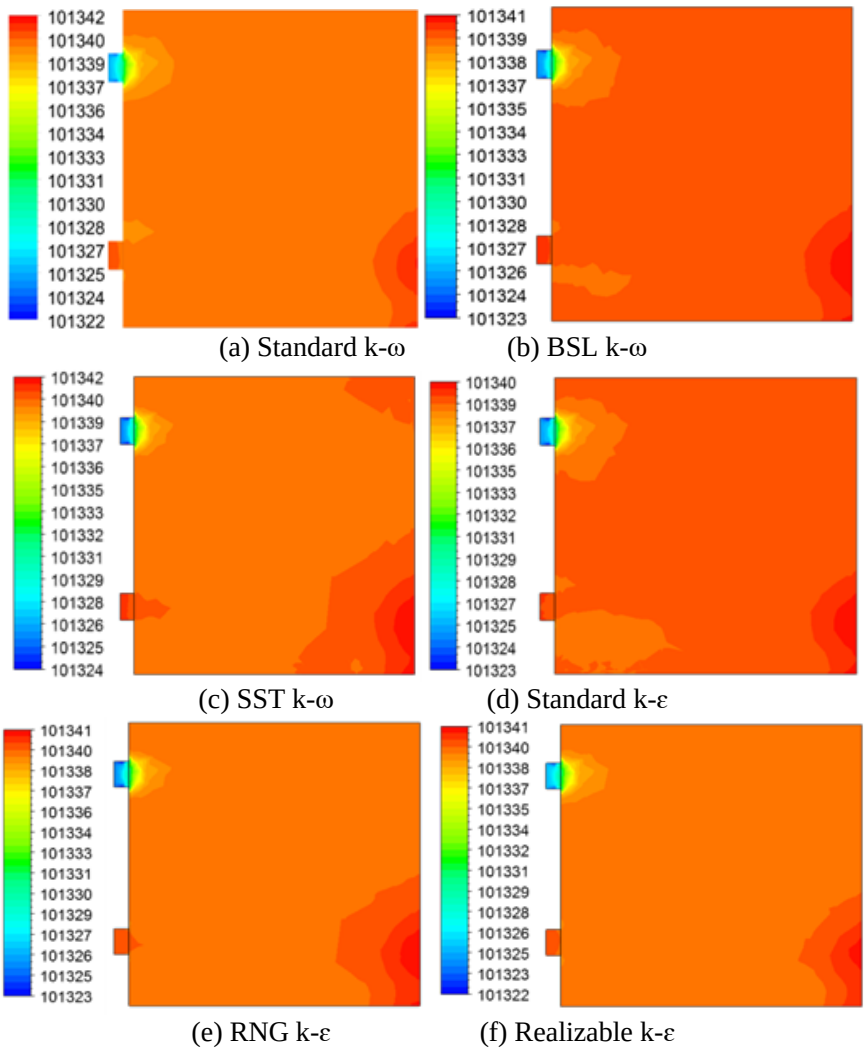

Figure 7. Distribution of the total pressure.

4.4. Turbulent Kinetic Energy

Figure 8 depicts the distribution of the turbulent kinetic energy in the plane defined by x = 0.06 m for the considered turbulence models. From these results, it can be seen that the turbulent kinetic energy presents a small value at the system inlet. In mean time, the turbulent kinetic energy increases

COMPLIMENTARY COPY

gradually in the expulsion area created in the down hole of the box. Otherwise, it has been observed that the maximum values of the turbulent kinetic energy appear at the discharge area near the reverse wall and at the top hole of the box outlet. As causes the other air proprieties, this fact is owing to the recirculation zone in the whole area of the box.

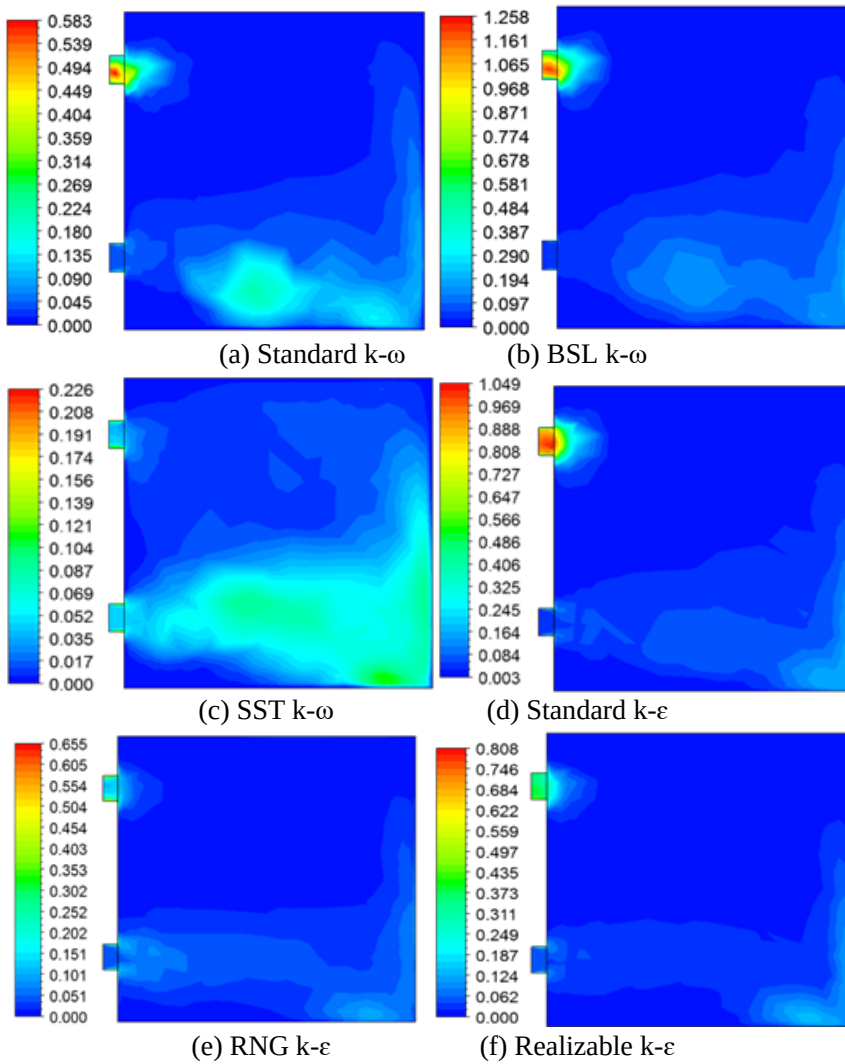

Figure 8. Distribution of the turbulent kinetic energy.

COMPLIMENTARY COPY

Indeed, the distribution of the turbulent kinetic energy in the four considered turbulence models affirms that the turbulence model presents a straight effect on the distribution of the turbulent kinetic energy. In fact, it has been observed that the maximum value of the turbulent kinetic energy is obtained in the hole outlet and it reaches $k = 1.258\ m^2.s^{-2}$ for the BSL k-ω turbulence model. However, this value reaches a low value, which is about $k = 0.226\ m^2.s^{-2}$, for the SST k-ω turbulence model.

4.5. Turbulent Viscosity

Figure 9 shows the distribution of the turbulent viscosity in the plane defined by x = 0.06 m and for the four turbulence models. According to these results, it can be seen that the turbulent viscosity presents a small value at the box inlet for all cases. However, the turbulent viscosity rises at the expulsion area which shown in the down hole of the system. The maximum values of the turbulent viscosity appear in the discharge area near the reverse wall. Otherwise, a peak value appears at the top hole of the box prototype due to the recirculation zone of the hot air in this region. By comparison of the obtained results, it has been observed a small effect of the different studied models on the distribution of the turbulent viscosity. In fact, the extension of the wake zone distinctiveness of the maximum values of the turbulent viscosity, obtained in the discharge area near the reverse wall, is more developed for the BSL k-ω turbulence model. Using this model, the maximum value of the turbulent viscosity reaches $\mu_t = 0.00192\ kg.m^{-1}.s^{-1}$ in the hole outlet. However, this parameter presents a low value equal to $\mu_t = 0.00032\ kg.m^{-1}.s^{-1}$ for the RNG k-ε turbulence model in the discharge area. In this case, the turbulent viscosity continues to decrease immensely in the outlet hole.

Conclusion

The present paper aims to investigate the impact of the turbulent model on the heat ventilation studied in a box prototype. Particularly, a computational study and an experimental validation have been developed to compare the standard k-ω, the SST k-ω, the BSL k-ω, the standard k-ε, the Realizable k-ε and the the RNG k-ε turbulence models. From the obtained results, it is noticed that the aerodynamic characteristics presents the same emergence nevertheless the

COMPLIMENTARY COPY

maximum values depend on the turbulence model. Particularly, it has been noted that the value founded with the standard k-ω tubulence model is nearest to the experimental data. This study tends to show that the standard k-ω turbulence model is the most efficient model to analyze the air flow in the box prototype. In the future, we suggest to extend this application with others geometrical arrangements.

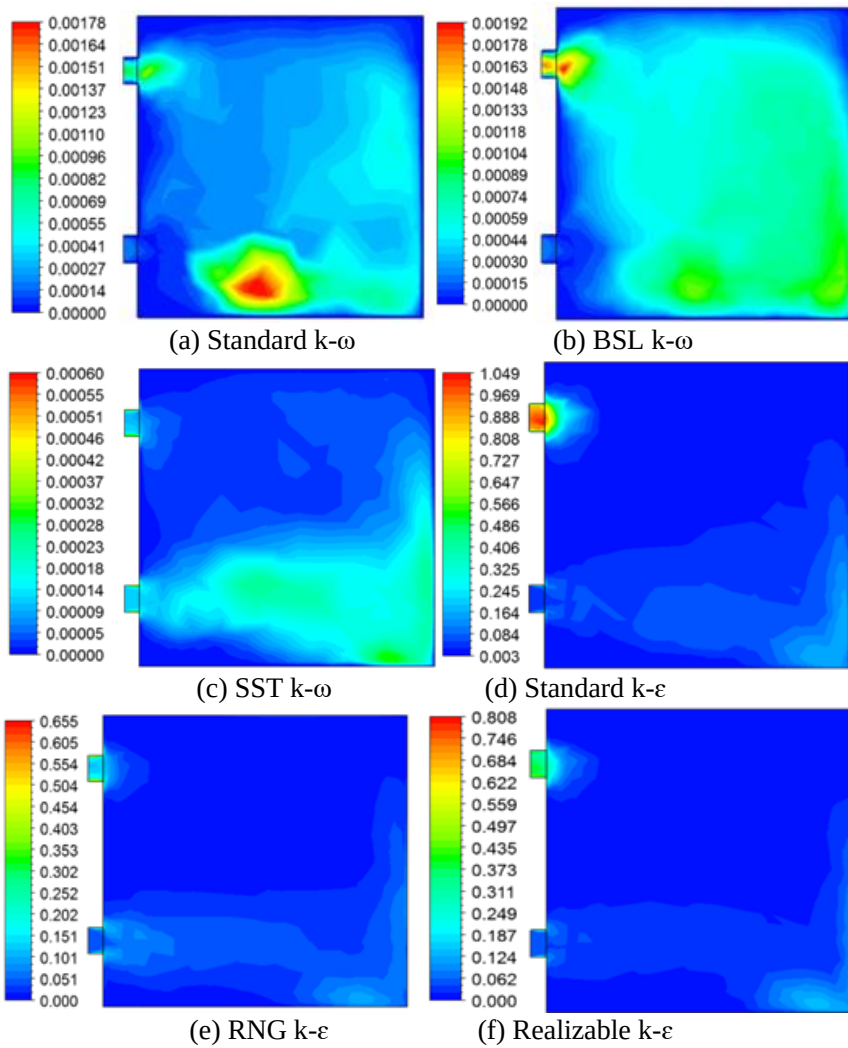

Figure 9. Distribution of the turbulent viscosity.

COMPLIMENTARY COPY

References

[1] S. Driss, Z. Driss, I. Kammoun, computational study and experimental validation of the heat ventilation in a living room with a solar patio system, *Energy and Building*, 119 (2016) 28-40.

[2] A. Ayadi, Z. Driss, A. Bouabidi, H. Nasraoui, M. Bsisa, M. S. Abid, A computational and an experimental study on the effect of the chimney height on the thermal characteristics of a solar chimney power plant, *Journal of Process Mechanical Engineering*, 231 (2017) 1-14.

[3] S. Driss, Z. Driss, I. Kammoun, Numerical simulation and wind tunnel experiments on wind-induced natural ventilation in isolated building with patio, *Energy*, 90 (2015) 917-925.

[4] H. Benguesmia, B. Bakri, Z. Driss, Effect of the turbulence model on the heat ventilation analysis in a box prototype, *Diagnostyka*, 21(3) (2020), 55-66.

[5] B. Bakri, S. Driss, A. Ketata, Z. Driss, H. Benguesmia, F. Hamrit, Study of the heat ventilation in a box prototype with the k-ω turbulence model, *Transylvanian Review Journal*, Vol XXXVI (30) (2018)7989-8000.

[6] B. Bakri, O. Eleuch, A. Ketata, S. Driss, Z. Driss, H. Benguesmia, Study of the turbulent flow in a newly solar air heater test bench with natural and forced convection modes, *Energy*, 161(2018)1028-1041.

[7] B. Bakri, A. Ketata, S. Driss, H. Benguesmia, Z. Driss, F. Hamrit, Unsteady investigation of the heat ventilation in a box prototype, *International Journal of Thermal Sciences*, 135 (2019)285-297.

[8] C. Teodosiu, F. Kuznik, R. Teodosiu, CFD modeling of buoyancy driven cavities with internal heat source: Application to heated rooms, 68 (2014) 403-411.

[9] X. Du, R. Bokel, A. V. D. Dobbelsteen, Building microclimate and summer thermal comfort in free-running buildings with diverse spaces: a Chinese vernacular house case, *Build. Environ.*, 822 (2014) 15-227.

[10] R. Z. Homod, Assessment regarding energy saving and decoupling for different AHU (air handling unit) and control strategies in the hot-humid climatic region of Iraq, *Energy*, 74 (2014) 762-774.

[11] F. J. Terrados, D. Moreno, "Patio" and "Botijo": Energetic strategies' architectural integration in"Patio 2.12" prototype. *Energy and Buildings*, 83 (2014) 70-88.

[12] E. Yasa, Microclimatic comfort measurements evaluation of building physics: The effect of building form and building settled area, on pedestrian level comfort around buildings, *Journal of Building Physics*, 40 (2016) 472-500.

[13] M. Premrov, V. Z. Leskovar, K. Mihalic, Influence of the building shape on the energy performance of timber-glass buildings in different climatic conditions, *Energy*, 108 (2016) 201-211.

[14] D. Johnston, Dominic Miles-Shenton, David Farmer, Quantifying the domestic building fabric 'performance gap,' *Building Services Engineering Research and Technology*, 36 (2015) 614-627.

[15] A. L. S. Chan, Investigation on the appropriate floor level of residential building for installing balcony, from a view point of energy and environmental performance. A case study in subtropical Hong Kong, *Energy*, 85 (2015) 620-634.

COMPLIMENTARY COPY

[16] M. Ibrahim, E. Wurtz, P. H. Biwole, P. Achard, Transferring the south solar energy to the north facade through embedded water pipes, *Energy*, 78 (2014) 834-845.
[17] Y. Nam, H. B. Chae, Numerical simulation for the optimum design of ground source heat pump system using building foundation as horizontal heat exchanger, *Energy*, 73 (2014) 933-942.
[18] M. R. Alam, M. F. M. Zain, A. B. M. A. Kaish, M. Jamil, Underground soil and thermal conductivity materials based heat reduction for energy-efficient building in tropical environment, *Indoor and Built Environment*, 24 (2013) 185-200.
[19] C. Rode, Global building physics, *Journal of Building Physics*, 36 (2012) 337-352.
[20] H. J. Han, Y. I. Jeon, S. H. Lim, W. W. Kim, K. Chen, New developments in illumination, heating and cooling technologies for energy-efficient buildings, *Energy*, 35 (2010) 2647-2653.
[21] K. J. Watson, J. Evans, A. Karvonen, T. Whitley, Re-conceiving building design quality: A review of building users in their social context, *Indoor and Built Environment*, 25 (2014) 509-523.
[22] D. J. Sailor, T. B. Elley, M. Gibson, Exploring the building energy impacts of green roof design decisions - a modeling study of buildings in four distinct climates, *Journal of Building Physics*, 35 (2011) 372-391.
[23] B. Bakri, S. Driss, A. Ketata, H. Benguesmia, F. Hamrit, Z. Driss, Study of the meshing effect on the turbulent flow in a building system with a k-ω turbulence model. *International Conference on Mechanics and Energy (ICME'2016)*, December 22-24 2016, Hammamet, Tunisia.
[24] B. Bakri, A. Ketata, S. Driss, H. Benguesmia, F. Hamrit, Z. Driss, Effect of the turbulence model on the aerodynamic structure to evaluate the thermal comfort in a building system, *International Conference on Mechanics and Energy (ICME'2016)*, December 22-24 2016, Hammamet, Tunisia.
[25] B. Bakri, A. Ketata, S. Driss, Z. Driss, H. Benguesmia, F. Hamrit, Unsteady simulation of the aerodynamic structure in a heated box prototype, *International Conference on Mechanics and Energy (ICME'2017)*, December 18-20 2017, Sousse, Tunisia.
[26] B. Bakri, S. Driss, A. Ketata, Z. Driss, H. Benguesmia, F. Hamrit, Study of the turbulent flow in a box prototype with the k-ω turbulence model, *Congrès Algérien de Mécanique, (CAM2017-289)*, 26-30 Novembre, Constantine-Algérie.
[27] B. Bakri, H. Benguesmia, A. Ketata, S. Driss, Z. Driss, F. Hamrit, Study of the natural convection flow in a solar air heater test bench, *International Conference on Mechanics and Energy (ICME'2018)*, December 20-22 2018, Hammamet, Tunisia.
[28] B. Bakri, H. Benguesmia, A. Ketata, H. Nasraoui, Z. Driss, Performance evaluation of the natural-convection of a solar air-heater with a plate absorber, *International Conference on Mechanics and Energy (ICME'2018)*, December 19-21 2019, Monastir, Tunisia.
[29] B. Bakri, H. Benguesmia, Study of the forced convective heat transfer in a solar air heater, *The First International Conference on Materials, Energy and Environment (MEE'2020, N°: EO05)*, January 20-21, 2020, El Oued University, Algeria.
[30] B. Bakri, H. Benguesmia, A. Ketata, S. Driss, Z. Driss, A comparative study of the turbulence models on the heat ventilation in a box prototype, *1ère Conférence*

COMPLIMENTARY COPY

National sur: la Transition Énergétique en Algérie Conférence (CNTEA1-2020), Mars 8-9, 2020, M'sila, Algeria.

[31] B. Bakri, H. Benguesmia, A. Ketata, S. Driss, Z. Driss, Choice of the appropriate turbulence model for modeling the air flow inside a room, *1ère Conférence National sur: la Transition Énergétique en Algérie Conférence (CNTEA1-2020)*, Mars 8-9, 2020, M'sila, Algeria.

[32] B. Bakri, H. Benguesmia, A. Ketata, S. Driss, Z. Driss, CFD Based performance analysis of a solar air heater test bench with unsteady turbulent flow, *9ème Journées des sciences de l'ingénieur JSI'2020*, September 25-27, 2020, Sfax, Tunisia.

[33] Z. Driss, O. Mlayeh, D. Driss, M. Maaloul, M. S. Abid, Numerical simulation and experimental validation of the turbulent flow around a small incurved Savonius wind rotor. *Energy*, 74 (2014) 506-517.

[34] Z. Driss, G. Bouzgarrou, W. Chtourou, H. Kchaou, M. S. Abid. Computational studies of the pitched blade turbines design effect on the stirred tank flow characteristics. *European Journal of Mechanics B/Fluids*, 29 (2010) 236-245.

[35] Z. Driss, O. Mlayah, S. Driss, M. Maaloul, M. S. Abid, Study of the incidence angle effect on the aerodynamic structure characteristics of an incurved Savonius wind rotor placed in a wind tunnel, *Energy*, 113 (2016) 894-908.

[36] Z. Driss, O. Mlayah, S. Driss, D. Driss, M. Maaloul, M. S. Abid, Study of the bucket design effect on the turbulent flow around unconventional Savonius wind rotors, *Energy*, 89 (2015) 708-729.

COMPLIMENTARY COPY